

Nonlinear Hall effect and scaling law in Sb-doped topological insulator MnBi₄Te₇

Shaoyu Wang¹, Xiubing Li¹, Heng Zhang¹, Bo Chen¹, Hangkai Xie¹, Congcong Li¹,
Fucong Fei², Shuai Zhang^{1,*} and Fengqi Song¹

¹ National Laboratory of Solid State Microstructures, Collaborative Innovation Center of Advanced Microstructures, and School of Physics, Nanjing University, Nanjing 210093, China

² National Laboratory of Solid State Microstructures, Collaborative Innovation Center of Advanced Microstructures, and School of Materials Science and Intelligent Engineering, Nanjing University, Suzhou 215163, China

* Corresponding author. Email: S.Z.(szhang@nju.edu.cn).

Abstract

Nonlinear Hall effect (NLHE), as a new member of Hall effect family, has been realized in many materials, attracting a great deal of attention. Here, we report the observation of NLHE in magnetic topological insulator Sb-doped MnBi_4Te_7 flakes. The NLHE generation efficiency can reach up to 0.06 V^{-1} , which is comparable to that observed in MnBi_2Te_4 . Differently, the NLHE can survive up to 200 K, much larger than the magnetic transition temperature. We further study the scaling behavior of the NLHE with longitudinal conductivity. The linear relationship with opposite slope when temperature is below and above the magnetic transition temperature is uncovered. It reveals that the NLHE originates from skew scattering. Our work provides a platform to search NLHE with larger generation efficiency at higher temperatures.

The Hall effect refers to the phenomenon that a voltage is generated perpendicular to the direction of the current when a current is applied in a longitudinal direction. The traditional Hall effect requires either an applied magnetic field or an internal magnetic moment to break the time-reversal symmetry (TRS)¹⁻³. However, recent studies have found that in the non-centrosymmetric quantum materials with time-reversal symmetry, a second-harmonic transverse voltage can be observed, which scales quadratically with the longitudinal current⁴⁻⁶. It is called the nonlinear Hall effect (NLHE), and has great potential application in frequency doubling and rectification⁷⁻¹⁰. The NLHE was first discovered in Weyl semimetal WTe₂ thin films¹¹, and has been found in several kinds of quantum materials in recent years⁸⁻²¹. The origin of NLHE can be intrinsic Berry curvature dipole (BCD)¹¹⁻¹⁵, or extrinsic side jump and skew scattering^{10,17-20}. Additionally, there are several other kinds of nonlinear behavior on Hall effect, such as nonlinear planar Hall effect²² and nonlinear spin Hall effect²³. At present, the research on NLHE focuses not only on stronger nonlinear signals, but also higher operating temperatures of nonlinear phenomena^{8-10,21}.

The nonlinear transport in topological insulators (TIs) has attracted lots of interests. Recently, NLHE induced by quantum metric has been observed in antiferromagnetic TI MnBi₂Te₄ devices^{24,25}, which arises much attentions²⁶. But it only exists below the Néel temperature (T_N). Also, in nonmagnetic TI Bi₂Se₃ with threefold rotational symmetry, scattering induced NLHE was reported¹⁸. Although it can survive at higher temperature, the magnitude of NLHE is typically small. MnBi₄Te₇, as a member of MnBi₂Te₄ family, is consist of MnBi₂Te₄ layer and Bi₂Te₃ layer superlattice²⁷⁻²⁹. Compared to MnBi₂Te₄,

the intercalation of the Bi_2Te_3 layer in MnBi_4Te_7 reduces the interlayer antiferromagnetic (AFM) coupling²⁸⁻³⁰. And there is a smaller energy difference between the ferromagnetic (FM) state and AFM state^{28,31} in MnBi_4Te_7 . Moreover, the FM ground state can be realized by doping Sb³²⁻³⁴. Additionally, the symmetry of the Sb-doped MnBi_4Te_7 bulk crystal is lowered, which results in a chiral structure³⁴. Therefore, the Sb-doped MnBi_4Te_7 provides a suitable platform for exploring large nonlinear transport phenomena at higher temperature.

In this work, we observe the NLHE in the $\text{Mn}(\text{Bi}_{1-x}\text{Sb}_x)_4\text{Te}_7$ ($x \approx 0.3$) nanoflakes. The nonlinear Hall response is extremely remarkable at low temperatures. The NLHE generation efficiency η is comparable to that in MnBi_2Te_4 devices^{24,25}. And the signal persists up to 200 K, which is much larger than the magnetic critical temperature (T_C) 13 K^{28-30,32} of $\text{Mn}(\text{Bi}_{1-x}\text{Sb}_x)_4\text{Te}_7$. Additionally, the scaling law of NLHE changes sign when temperature is larger than T_C . And the linear scaling law indicates that NLHE primarily arises from the skew scattering.

The Sb-doped MnBi_4Te_7 crystals are grown using the flux method. The left part of Fig. 1(a) illustrates the crystal structure of Sb-doped MnBi_4Te_7 . The superlattice stacks along the c-axis through weak van der Waals forces. Compared to MnBi_4Te_7 , Sb and Bi atoms mix on the Bi site in $\text{Mn}(\text{Bi}_{1-x}\text{Sb}_x)_4\text{Te}_7$ sample^{32,34}. The magnetic transition of the crystal is related to Mn atoms. We chose the doping level $x = 0.3$ due to its FM ground state³². The $\text{Mn}(\text{Bi}_{0.7}\text{Sb}_{0.3})_4\text{Te}_7$ (MBST) nanoflakes were mechanically exfoliated from bulk crystals onto SiO_2/Si substrates. The electrode pattern was defined using electron

beam lithography, followed by the evaporation of Au film. The right part of Fig. 1(a) is the optical image of the device. The white scale bar is 20 μm . The height of the MBST nanoflake is around 20 nm, measured by atomic force microscopy. The transport measurements were conducted in the Physical Property Measurement System (PPMS). We utilized lock-in technique to measure the first- and second-harmonic transport signals.

Temperature-dependent longitudinal resistance (R_{xx}) is shown in Fig. 1(b). With temperature decreasing, the resistance increases first and then decreases. At low temperature, there is an upturn, which is probably due to the carrier localization in the presence of disorder^{35,36}. The magneto-resistances at various temperatures are shown in Fig. 1(c) and (d). From the linear fitting of Hall resistance (R_{xy}) in Fig. 1(d), we can obtain the carrier density n_{2D} approximately $\sim 10^{16} \text{ cm}^{-2}$. And the negative slope indicates an n -type carrier. Also, the anomalous Hall effect (AHE) with hysteresis loop can be observed under low temperature in Fig. 1(d), accompanied by the butterfly-shaped hysteresis in Fig. 1(c). It indicates the ferromagnetic phases at low temperature. The AHE diminishes gradually with the temperature increasing, consistent with the reported magnetic transition temperature $\sim 13 \text{ K}$.

Then we measured the I - V transport with a frequency of 37 Hz at various temperatures. Here, we show the typical transport properties below and above T_C in Fig. 2, i.e. $T = 2 \text{ K}$ and 20 K . Figure 2(a, d) is the current-dependent first harmonic longitudinal voltage V_{xx} at $T = 2 \text{ K}$ and 20 K , respectively. The linear I - V_{xx} curves indicate the Ohmic contact. The second harmonic I - $V^{2\omega}$ curve is shown in Fig. 2(b, e).

The red and black dots are second harmonic Hall voltage $V_{xy}^{2\omega}$ and longitudinal voltage $V_{xx}^{2\omega}$, respectively. The solid line represents a quadratic fit to current, which satisfies the NLHE relationship $V_{xy}^{2\omega} \propto I^2$. When $I = 4.8 \mu\text{A}$, $V_{xy}^{2\omega}$ can reach $-21 \mu\text{V}$ at 2 K. It is about 0.1% of the magnitude of V_{xx} . But the magnitude of $V_{xx}^{2\omega}$ is significantly smaller than $V_{xy}^{2\omega}$. It rules out the possibility of the mixing of second harmonic Hall voltage and longitudinal voltage. Importantly, we can find that the NLHE exhibits both below and above T_C . It is different from the NLHE in MnBi_2Te_4 , which only exists below the magnetic transition temperature^{24,25}. Compared to Sb-doped MnBi_4Te_7 , NLHE in pure MnBi_4Te_7 is negligibly small (Fig. S1).

To further confirm the NLHE, we measured the second harmonic transport with the reversal of the source and drain and the corresponding Hall probes, as illustrated in the inset of Fig. 2(c, f). We can find that $V_{xy}^{2\omega}$ would change the sign when the current direction reverses, while the magnitude of NLHE is almost unchanged. Also, $V_{xx}^{2\omega}$ exhibits similar behavior as $V_{xy}^{2\omega}$ (Fig. S2). It is distinct from the behavior of conventional Hall effect. And the heating effect can be excluded¹⁶.

The temperature dependent $V_{xy}^{2\omega}$ at $I = 4.8 \mu\text{A}$ is shown in Fig. 3(a). The magnitude of NLHE decreases as the temperature increases, with a kink around T_C . It can exist up to 200 K, much larger than the magnetic critical temperature. It is different from the previous reported NLHE^{24,25} in MnBi_2Te_4 , which would disappear when the temperature is over T_N . At high temperature, the magnitude of NLHE decreases slowly as T increases. Different from^{24,25} MnBi_2Te_4 , Sb-doped MnBi_4Te_7 has a chiral structure without inversion symmetry³⁴. It may lead to the existence of NLHE over T_C . We also

measured the NLHE with different frequencies. As shown in Fig. 3(b), the nonlinear Hall responses as a function of I at three different frequencies (23 Hz, 37 Hz and 43Hz) coincide with each other. It can rule out the possibility of spurious capacitive coupling effect^{11,12,16}.

Since $V_{xy}^{2\omega}$ is proportional to the square of current, and V_{xx} scales linearly with the current, we use $\eta = |V_{xy}^{2\omega}|/(V_{xx})^2$ to characterize the strength of NLHE, which can be called NLHE generation efficiency¹². Figure 4(a) shows the temperature dependence of η . At low temperature, the generation efficiency η can reaches 0.06 V^{-1} . Compared with recent works in MnBi_2Te_4 ^{24,25}, it is in the same order of magnitude. With temperature increasing, η gradually decreases. But it is larger than 0.02 V^{-1} when temperature is below 60 K, without an order of magnitude reduction. Moreover, η is four orders of magnitude larger than that in TI¹⁸ Bi_2Se_3 . The NLHE compared to recent works in (magnetic) TIs^{18,24,25} is shown in Fig. 4(d) (see more details in Table S1), which demonstrates the high performance of this work.

Then, we discuss the physical origin of the NLHE. Similar to AHE^{2,37,38}, a scaling law can be used to distinguish different origins of NLHE³⁹⁻⁴². According to the theory, η scales linearly with σ_{xx}^2 , i.e. $\eta = A\sigma_{xx}^2 + B$, where the first part represents the contribution of disorder, and the second part is contributed by the intrinsic BCD. The temperature dependent σ_{xx} is shown in Fig. 4(b), with a turning point around T_C .

We plotted the values of η v.s. σ_{xx}^2 , and it is fitted by to the above equation, as shown in Fig. 4(c). Note that the temperature range can be divided into two different regions according to T_C ($\sim 13 \text{ K}$). In both regions, the experimental data can be fitted

well by the theoretical equation. The linear fitting in the two regions indicates that the skew scattering may be the main origin^{7,39-42}. Besides, the slope of the fitted line (A) is opposite. Above T_C , the time-reversal symmetry is unbroken. In this range, the slope is positive. This is consistent with the previous work in TI¹⁸. While the slope is negative below T_C , which may indicate that the contribution to skew scattering is different from that at high temperatures. The NLHE and intriguing scaling law is reproducible in another MBST device (Figs. S3 and S4). And the generation efficiency is on the order of 0.1 V^{-1} . Further study is needed to clarify the mechanism.

In conclusion, we demonstrate NLHE in Sb-doped MnBi_4Te_7 nanoflakes, which can persist up to a high temperature. The NLHE shows the linear scaling law with opposite slope in two different temperature ranges, which indicates the NLHE originates from skew scattering. Our work paves the way for searching larger NLHE at higher temperatures.

Acknowledgements

We gratefully acknowledge the financial support of the National Key R&D Program of China (No. 2022YFA1402404), the National Natural Science Foundation of China (Grant Nos. 92161201, T2221003, 12374043, 12274208, and 12025404).

References

1. D. Xiao, M.-C. Chang, and Q. Niu, “Berry phase effects on electronic properties,” *Rev. Mod. Phys.* **82**, 1959–2007 (2010).
2. N. Nagaosa, J. Sinova, S. Onoda, A. H. MacDonald, and N. P. Ong, “Anomalous Hall effect,” *Rev. Mod. Phys.* **82**, 1539–1592 (2010).
3. C. -Z. Chang, J. Zhang, X. Feng, J. Shen, Z. Zhang, M. Guo, K. Li, Y. Ou, P. Wei, L.-L. Wang *et al.*, “Experimental Observation of the Quantum Anomalous Hall Effect in a Magnetic Topological Insulator,” *Science* **340**, 167–170 (2013).
4. Sodemann, and L. Fu, “Quantum Nonlinear Hall Effect Induced by Berry Curvature Dipole in Time-Reversal Invariant Materials,” *Phys. Rev. Lett.* **115**, 216806 (2015).
5. C. Ortix, “Nonlinear Hall effect with time-reversal symmetry: theory and material realizations,” *Adv. Quantum Technol.* **4**, 2100056 (2021).
6. Z. Z. Du, C. M. Wang, H.-Z. Lu and X. C. Xie, “Band signatures for strong nonlinear Hall effect in bilayer WTe₂,” *Phys. Rev. Lett.* **121**, 266601 (2018).
7. H. Isobe, S.-Y. Xu, and L. Fu, “High-frequency rectification via chiral Bloch electrons,” *Sci. Adv.* **6**, eaay2497 (2020).
8. D. Kumar, C.-H. Hsu, R. Sharma, T.-R. Chang, P. Yu, J. Wang, G. Eda, G. Liang, and H. Yang, “Room-temperature nonlinear Hall effect and wireless radiofrequency rectification in Weyl semimetal TaIrTe₄,” *Nat. Nanotechnol.* **16**, 421–425(2021).
9. L. Min, H. Tan, Z. Xie, L. Miao, R. Zhang, S. H. Lee, V. Gopalan, C.-X. Liu, N. Alem, B. Yan *et al.*, “Strong room-temperature bulk nonlinear Hall effect in a spin-valley locked Dirac material,” *Nat. Commun.* **14**, 364 (2023).

10. X. F. Lu, C.-P. Zhang, N. Wang, D. Zhao, X. Zhou, W. Gao, X. H. Chen, K. T. Law, and K. P. Loh, “Nonlinear transport and radio frequency rectification in BiTeBr at room temperature,” *Nat. Commun.* **15**, 245 (2024).
11. Q. Ma, S.-Y. Xu, H. Shen, D. MacNeill, V. Fatemi, T.-R. Chang, A. M. M. Valdivia, S. Wu, Z. Du, C.-H. Hsu *et al.*, “Observation of the nonlinear Hall effect under time-reversal-symmetric conditions,” *Nature* **565**, 337 (2019).
12. M. Huang, Z. Wu, J. Hu, X. Cai, E. Li, L. An, X. Feng, Z. Ye, N. Lin, K. T. Law *et al.*, “Giant nonlinear Hall effect in twisted bilayer WSe₂,” *Natl. Sci. Rev.* **10**, nwac232 (2023).
13. S.-C. Ho, C.-H. Chang, Y.-C. Hsieh, S.-T. Lo, B. Huang, T.-H.-Y. Vu, C. Ortix, and T.-M. Chen, “Hall effects in artificially corrugated bilayer graphene without breaking time-reversal symmetry,” *Nat. Electron.* **4**, 116–125 (2021).
14. M.-S. Qin, P.-F. Zhu, X.-G. Ye, W.-Z. Xu, Z.-H. Song, J. Liang, K. Liu, and Z.-M. Liao, “Strain Tunable Berry Curvature Dipole, Orbital Magnetization and Nonlinear Hall Effect in WSe₂ Monolayer,” *Chinese Phys. Lett.* **38**, 017301(2021).
15. C.-L. Zhang, T. Liang, Y. Kaneko, N. Nagaosa, and Y. Tokura, “Giant Berry curvature dipole density in a ferroelectric Weyl semimetal,” *npj Quantum Mater.* **7**, 103 (2022).
16. K. Kang, T. Li, E. Sohn, J. Shan, and K. F. Mak, “Nonlinear anomalous Hall effect in few-layer WTe₂,” *Nat. Mater.* **18**, 324–328 (2019).
17. Tiwari, F. Chen, S. Zhong, E. Drueke, J. Koo, A. Kaczmarek, C. Xiao, J. Gao, X. Luo, Q. Niu *et al.*, “Giant c-axis nonlinear anomalous Hall effect in T_d-MoTe₂ and WTe₂,” *Nat. Commun.* **12**, 2049 (2021).

18. P. He, H. Isobe, D. Zhu, C.-H. Hsu, L. Fu, and H. Yang, “Quantum frequency doubling in the topological insulator Bi₂Se₃,” *Nat. Commun.* **12**, 698 (2021).
19. J. Duan, Y. Jian, Y. Gao, H. Peng, J. Zhong, Q. Feng, J. Mao, and Y. Yao, “Giant Second-Order Nonlinear Hall Effect in Twisted Bilayer Graphene,” *Phys. Rev. Lett.* **129**, 186801(2022).
20. P. He, G. K. W. Koon, H. Isobe, J. Y. Tan, J. Hu, A. H. C. Neto, L. Fu, and H. Yang, “Graphene moiré superlattices with giant quantum nonlinearity of chiral Bloch electrons,” *Nat. Nanotechnol.* **17**, 378–383 (2022).
21. P. Makushko, S. Kovalev, Yevhen Zabala, Igor Ilyakov, A. Ponomaryov, A. Arshad, G. L. Prajapati, T. V. A. G. de Oliveira, J.-C. Deinert, P. Chekhonin *et al.*, “A tunable room-temperature nonlinear Hall effect in elemental bismuth thin films,” *Nat Electron* (2024).
22. P. He, S. S.-L. Zhang, D. Zhu, S. Shi, O. G. Heinonen, G. Vignale, and H. Yang, “Nonlinear Planar Hall Effect,” *Phys. Rev. Lett.* **123**, 016801 (2019).
23. S. Hayami, M. Yatsushiro, and H. Kusunose, “Nonlinear spin Hall effect in *PT*-symmetric collinear magnets,” *Phys. Rev. B* **106**, 024405 (2022).
24. N. Wang, D. Kaplan, Z. Zhang, T. Holder, N. Cao, A. Wang, X. Zhou, F. Zhou, Z. Jiang, C. Zhang *et al.*, “Quantum-metric-induced nonlinear transport in a topological antiferromagnet,” *Nature* **621**, 487–492 (2023).
25. Gao, Y.-F. Liu, J.-X. Qiu, B. Ghosh, T. Trevisan, Y. Onishi, C. Hu, T. Qian, H.-J. Tien, S.-W. Chen *et al.*, “Quantum metric nonlinear Hall effect in a topological antiferromagnetic heterostructure,” *Science* **381**, 181-186(2023).
26. D. Kaplan, T. Holder, and B. Yan, “Unification of Nonlinear Anomalous Hall Effect

- and Nonreciprocal Magnetoresistance in Metals by the Quantum Geometry,” *Phys. Rev. Lett.* **132**, 026301(2024).
27. H.-K. Xu, M. Gu, F. Fei, Y.-S. Gu, D. Liu, Q.-Y. Yu, S.-S. Xue, X.-H. Ning, B. Chen, H. Xie *et al.*, “Observation of Magnetism-Induced Topological Edge State in Antiferromagnetic Topological Insulator MnBi_4Te_7 ,” *ACS Nano* **16**, 9810-9818 (2022).
 28. H. Xie, D. Wang, Z. Cai, B. Chen, J. Guo, M. Naveed, S. Zhang, M. Zhang, X. Wang, F. Fei *et al.*, “The mechanism exploration for zero-field ferromagnetism in intrinsic topological insulator MnBi_2Te_4 by Bi_2Te_3 intercalations,” *Appl. Phys. Lett.* **116**, 221902 (2020).
 29. M. Z. Shi, B. Lei, C. S. Zhu, D. H. Ma, J. H. Cui, Z. L. Sun, J. J. Ying, and X. H. Chen, “Magnetic and transport properties in the magnetic topological insulators $\text{MnBi}_2\text{Te}_4(\text{Bi}_2\text{Te}_3)_n$ ($n=1,2$),” *Phys. Rev. B* **100**, 155144 (2019).
 30. J.-Q. Yan, Y. H. Liu, D. S. Parker, Y. Wu, A. A. Aczel, M. Matsuda, M. A. McGuire, and B. C. Sales, “A-type antiferromagnetic order in MnBi_4Te_7 and $\text{MnBi}_6\text{Te}_{10}$ single crystals,” *Phys. Rev. Materials* **4**, 054202(2020).
 31. L. Ding, C. Hu, F. Ye, E. Feng, N. Ni, and H. Cao, “Crystal and magnetic structures of magnetic topological insulators MnBi_2Te_4 and MnBi_4Te_7 ,” *Phys. Rev. B* **101**, 020412 (2020).
 32. B. Chen, D. Wang, Z. Jiang, B. Zhang, S. Cui, J. Guo, H. Xie, Y. Zhang, M. Naveed, Y. Du *et al.*, “Coexistence of ferromagnetism and topology by charge carrier engineering in the intrinsic magnetic topological insulator MnBi_4Te_7 ,” *Phys. Rev. B* **104**, 075134(2021).

33. C. Hu, S.-W. Lien, E. Feng, S. Mackey, H.-J. Tien, I. I. Mazin, H. Cao, T.-R. Chang, and N. Ni, "Tuning magnetism and band topology through antisite defects in Sb-doped MnBi_4Te_7 ," *Phys. Rev. B* **104**, 054422 (2021).
34. Y. D. Guan, C. H. Yan, S. H. Lee, X. Gui, W. Ning, J. L. Ning, Y. L. Zhu, M. Kothakonda, C. Q. Xu, X. L. Ke *et al.*, "Ferromagnetic MnBi_4Te_7 obtained with low-concentration Sb doping: A promising platform for exploring topological quantum states," *Phys. Rev. Materials* **6**, 054203(2022).
35. Y. Deng, Y. Yu, M. Z. Shi, Z. Guo, Z. Xu, J. Wang, X. H. Chen, and Y. Zhang, "Quantum anomalous Hall effect in intrinsic magnetic topological insulator MnBi_2Te_4 ," *Science* **367**, 895-900 (2020).
36. J. Ge, Y. Liu, J. Li, H. Li, T. Luo, Y. Wu, Y. Xu, and J. Wang, "High-Chern-number and high-temperature quantum Hall effect without Landau levels," *Natl. Sci. Rev.* **7**, 1280 (2020).
37. Y. Tian, L. Ye, and X. Jin, "Proper scaling of the anomalous Hall effect," *Phys. Rev. Lett.* **103**, 087206 (2009).
38. D. Hou, G. Su, Y. Tian, X. Jin, S. A. Yang, and Q. Niu, "Multivariable scaling for the anomalous Hall effect," *Phys. Rev. Lett.* **114**, 217203 (2015).
39. Z. Z. Du, C. M. Wang, S. Li, H.-Z. Lu, and X. C. Xie, "Disorder-induced nonlinear Hall effect with time-reversal symmetry," *Nat. Commun.* **10**, 3047 (2019).
40. Z.-F. Wu, M.-Z. Huang, and N. Wang, "Nonlinear Hall effects in two-dimensional moiré superlattices," *Acta Phys. Sin.* **2023**, 72(23):237301(2023).
41. C. Xiao, H. Zhou, and Q. Niu, "Scaling parameters in anomalous and nonlinear Hall

effects depend on temperature,” *Phys. Rev. B* **100**, 161403(2019).

- ⁴² Z. Z. Du, H.-Z. Lu, and X. C. Xie, “Nonlinear Hall Effect,” *Nat. Rev. Phys.* **3**, 744–752 (2021).

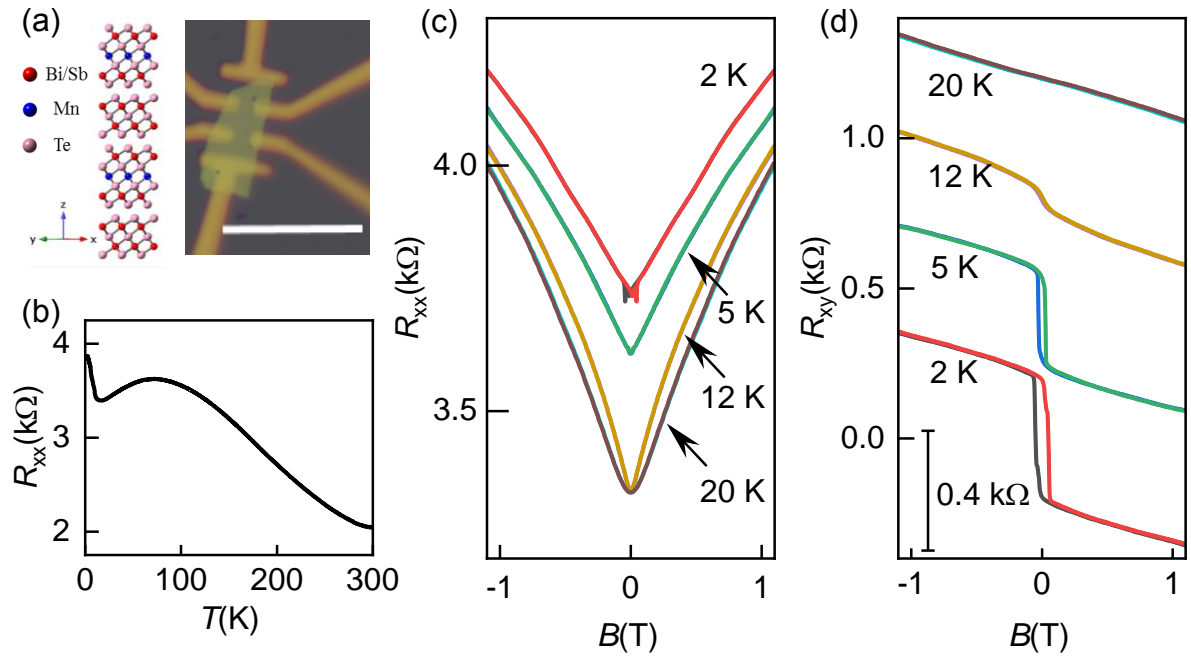


Figure 1. (a) Left part is the crystal structure of Sb-doped MnBi₄Te₇. Right part is the optical image of Mn(Bi_{1-x}Sb_x)₄Te₇ device. The white scale bar is 20 μ m. (b) Temperature dependent R_{xx} . (c) Magnetic field dependent R_{xx} at different temperatures. (d) Magnetic field dependent R_{xy} at different temperatures. The Hall resistances under different temperatures are shifted vertically.

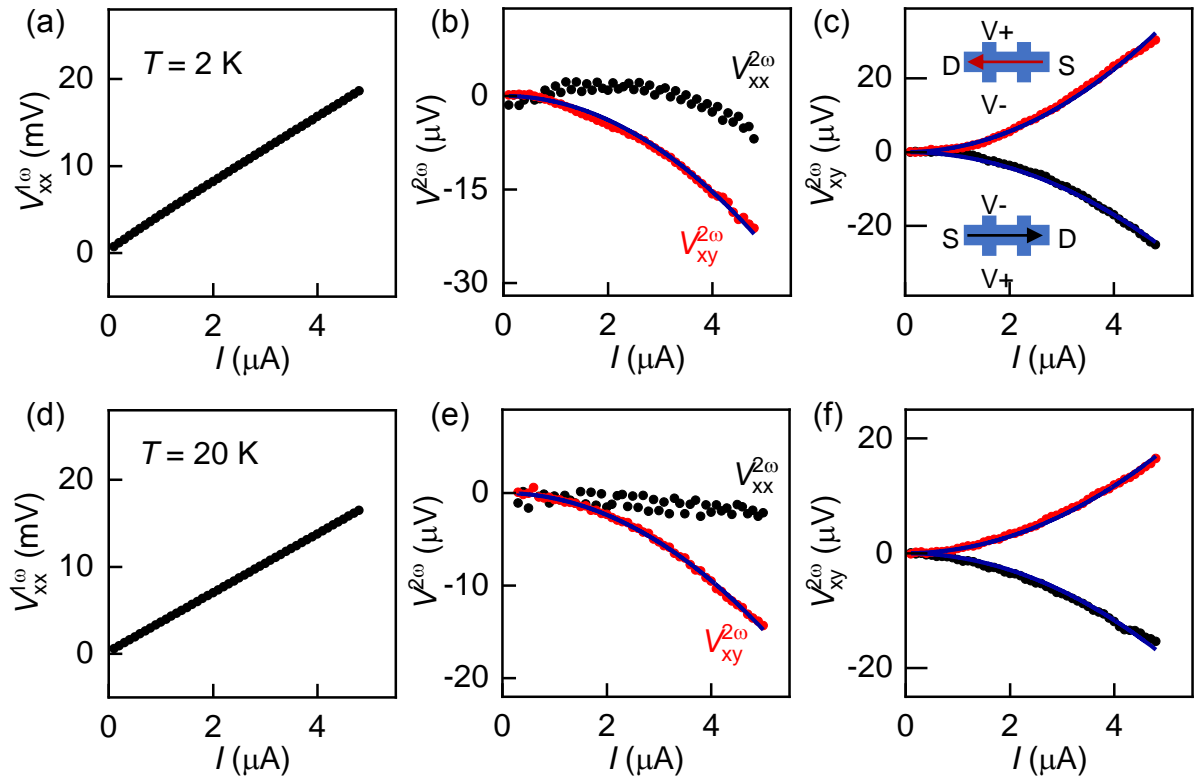


Figure 2. (a) Current dependent first harmonic longitudinal voltage V_{xx} of $\text{Mn}(\text{Bi}_{1-x}\text{Sb}_x)_4\text{Te}_7$ at 2 K. (b) Current dependent second harmonic longitudinal voltage $V_{xx}^{2\omega}$ and Hall voltage $V_{xy}^{2\omega}$. The solid line is a quadratic fit. (c) The nonlinear Hall voltage $V_{xy}^{2\omega}$ with the reversal of current direction. It changes the sign with reversing the current direction. (d-f) The same curves as (a-c) at 20 K.

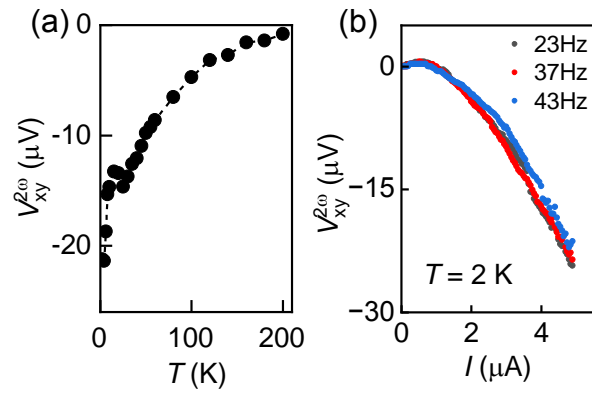


Figure 3. (a) Temperature dependent nonlinear Hall voltages at $I = 4.8 \mu\text{A}$. (b) Current dependent nonlinear Hall voltages with different driving frequencies.

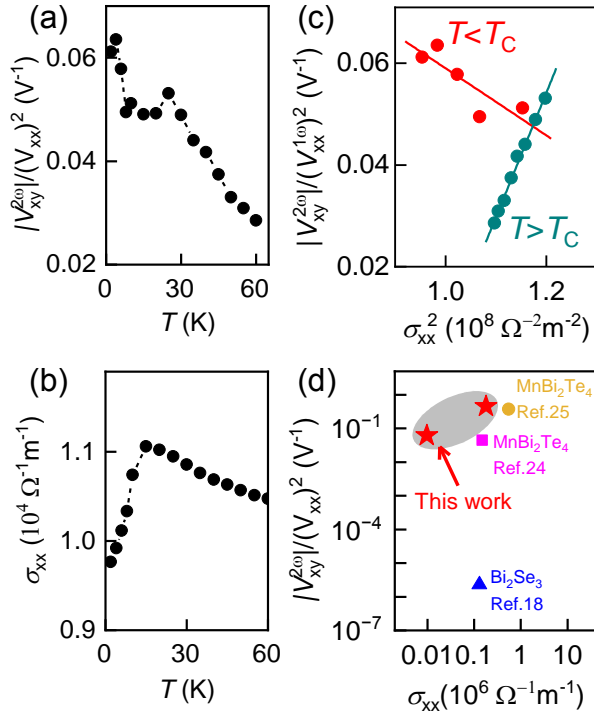


Figure 4. (a) Temperature dependent nonlinear Hall generation efficiency. (b) Temperature dependent longitudinal conductivity. (c) The scaling law of nonlinear Hall effect, $|V_{xy}^{2\omega}|/(V_{xx})^2 = A\sigma_{xx}^2 + B$. The solid lines are the linear fitting for different temperature ranges. (d) The nonlinear Hall effect compared to recent works in (magnetic) topological insulators.